NORGES TEKNISK-NATURVITENSKAPELIGE
UNIVERSITET

Efficient time-symmetric simulation of torqued rigid bodies using Jacobi elliptic functions.

by

Elena Celledoni and Niklas Säfström

PREPRINT
NUMERICS NO. 8/2005

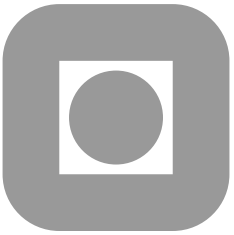

NORWEGIAN UNIVERSITY OF SCIENCE AND
TECHNOLOGY
TRONDHEIM, NORWAY

This report has URL
http://www.math.ntnu.no/preprint/numerics/2005/N8-2005.ps
Address: Department of Mathematical Sciences, Norwegian University of Science and Technology,
N-7491 Trondheim, Norway.

Abstract

If the three moments of inertia are different from each other, the solution to the free rigid body (FRB) equations of motion is given in terms of Jacobi elliptic functions. Using the Arithmetic-Geometric mean algorithm, [1], these functions can be calculated efficiently and accurately. The overall approach yields a faster and more accurate numerical solution to the FRB equations compared to standard numerical ODE and symplectic solvers. This approach performs well also for mass asymmetric rigid bodies.
In this paper we consider the case of rigid bodies subject to external forces. We consider a strategy similar to the symplectic splitting method proposed in [16]. The method here proposed is time-symmetric. We decompose the vector field of our problem in a FRB problem and another completely integrable vector field.
In our experiments we observe that the overall numerical solution benefits greatly from the very accurate solution of the FRB problem. We apply the method to the simulation of artificial satellite attitude dynamics.

1 Introduction

We consider the Euler equations describing the motion of a free rigid body (FRB),

$$\begin{aligned} I_1\dot{\omega}_1 &= (I_2 - I_3)\omega_2\omega_3, \\ I_2\dot{\omega}_2 &= (I_3 - I_1)\omega_3\omega_1, \\ I_3\dot{\omega}_3 &= (I_1 - I_2)\omega_1\omega_2, \end{aligned} \tag{1}$$

where I_1, I_2 and I_3 are the principal moments of inertia. These equations are completely integrable. Energy and angular momentum are preserved along the solution, this means that for all times the two quantities

$$E = I_1\omega_1^2 + I_2\omega_2^2 + I_3\omega_3^2, \quad G^2 = I_1^2\omega_1^2 + I_2^2\omega_2^2 + I_3^2\omega_3^2, \tag{2}$$

are constant, (here E is the energy and G^2 is the total angular momentum). There is also a non canonical symplectic structure preserved by the flow of (1), [11].

By using the two constants of motion it is possible to derive the general solution of the equations expressed in terms of Jacobi elliptic functions.

The expression of the exact general solution of the FRB equations can be turned into a numerical method by using efficient numerical approximations of the Jacobi elliptic functions. Some extra computational work is required to impose initial conditions. We also refer to [3] and [14] for related literature. In this paper we show how this approach is very competitive and we discuss the details of its further use in problems of rigid bodies subject to external forces.

The simulation of rigid body motion is interesting for applications in robotics, structural mechanics, and molecular dynamics, [7], [9].

Symplectic integration methods for the Euler equations have been constructed by various authors, [6], [15], [10], [13], see also [9] and references therein. Many of these methods cannot be straightforwardly generalized to the broader class of non canonical Hamiltonian problems, thus their use is limited to the numerical approximation of the FRB equations. However some of these numerical tools have successfully been applied in the simulation of rigid body dynamics and of torqued rigid bodies. In [16] and [2], a splitting method for the FRB equations has been successfully generalized into a symplectic splitting for the case of torqued rigid bodies.

For the FRB equations, in [12] and [16], the right hand side of (1) is split in the following three terms,

$$f_1(\omega) = \begin{bmatrix} 0 \\ I_3\omega_3\omega_1 \\ -I_2\omega_1\omega_2 \end{bmatrix}, \quad f_2(\omega) = \begin{bmatrix} -I_3\omega_2\omega_3 \\ 0 \\ I_1\omega_1\omega_2 \end{bmatrix}, \quad f_3(\omega) = \begin{bmatrix} I_2\omega_2\omega_3 \\ -I_1\omega_3\omega_1 \\ 0 \end{bmatrix}. \quad (3)$$

Each of the three vector fields is Hamiltonian, and defines a differential equation which is easy to integrate exactly. The appropriate composition of the corresponding flows produces a symplectic approximation of the problem. This symplectic method seems to outperform most of the known and previously proposed strategies of symplectic integration of the FRB problem, [4], [13]. We use this splitting for comparison in our numerical experiments. The generalization to the case of torqued rigid bodies, in [16], is achieved by considering a splitting of the Hamiltonian of the problem in four parts, three of them give rise to vector fields analogous to f_1, f_2 and f_3, the last vector field is completely integrable and arises form the potential energy yielding the torque. We will briefly recall this approach in section 4.

The method proposed in the present paper is time-symmetric, and related to the approach of [16] and and [2]. We decompose the vector field of our problem in a FRB problem and another completely integrable vector field. Even if the numerical approximation of the FRB equations is performed to machine accuracy, the overall splitting is not symplectic. However the loss of symplecticity does not seem to have significant influence on the qualitative performance of the new method. On the contrary in some experiments the new method presents considerably better conservation of energy and better behavior of the numerical solution.

Accurate, symplectic, energy and momentum preserving approximations for the solution of the FRB equations, have been recently addressed in [13]. In this work the authors propose a new implementation of the Discrete Moser-Veselov algorithm of [15], and achieve order four and six in the integration by applying appropriate rescaling of the initial condition. The rescaling need to be performed just once, at the beginning of the integration leading to a significant improvement with respect to the second order Discrete Moser-Veselov algorithm.

Our numerical tests show that using the exact solution and computing (14) to machine accuracy leads to a very competitive method also compared to the improved Discrete Moser-Veselov approach for the solution of the FRB equations. Both approaches require the computation of some quantities prior to the time stepping, the rescaling factors for the DMV, and the constants for imposing the initial condition in the case of the Jacobi elliptic functions. This implies increased computational cost when the methods are used within a splitting technique for torqued rigid bodies. Still the symmetric splitting method of this paper appears to be very competitive also in the case of torqued rigid bodies, at least in the presented experiments.

The outline of the paper is as follows. The new method is presented in section 2. Some technical issues for the implementation of this approach are discussed in section 3. In section 4 we report some numerical experiments comparing the proposed approach to the Discrete Moser Veselov approach of [13] and the symplectic splitting of [16], [2].

2 A symmetric splitting method for torqued rigid bodies

Efficient integrators for the free rigid body can be used in connection with splitting methods in the numerical approximation of more complex rigid body dynamics. The method pre-

sented here can also be applied to problems of interacting rigid bodies, rigid body linked by constrains, etc [2].

The Hamiltonian function for our problem is

$$\mathcal{H} = \mathcal{H}(\pi, Q) = \frac{1}{2}\left(\frac{\pi_1^2}{I_1} + \frac{\pi_2^2}{I_2} + \frac{\pi_3^2}{I_3}\right) + V(Q),$$

where $\pi = (I_1\omega_1, I_2\omega_2, I_3\omega_3)^T$ is the angular momentum and Q is the rotation matrix.

The Hamiltonian $\mathcal{H}$ gives rise to the following system of ordinary differential equations

$$\dot{\pi} = \text{skew}(T^{-1}\pi)\,\pi + f(Q), \tag{4}$$

$$\dot{Q} = \text{skew}(T^{-1}\pi)\,Q, \tag{5}$$

where

$$\text{skew}(v) = \begin{pmatrix} 0 & v_3 & -v_2 \\ -v_3 & 0 & v_1 \\ v_2 & -v_1 & 0 \end{pmatrix},$$

f depends on the potential energy $V(Q)$, and

$$T = \begin{pmatrix} I_1 & 0 & 0 \\ 0 & I_2 & 0 \\ 0 & 0 & I_3 \end{pmatrix}$$

is the inertia tensor. To derive a symmetric splitting method for the above equations, we start by applying a Störmer/Verlet splitting,

$$\mathcal{H} = \mathcal{H}_1 + \mathcal{H}_2, \quad \mathcal{H}_2 = V(Q),$$

and $\mathcal{H}_1 = \mathcal{H} - \mathcal{H}_2$ is the kinetic energy. The system of differential equation is then split into the two systems

$$S_1 = \begin{cases} \dot{\pi} = \text{skew}(T^{-1}\pi)\,\pi, \\ \dot{Q} = \text{skew}(T^{-1}\pi)\,Q, \end{cases} \tag{6}$$

with $\pi(t) = Q(t)\pi_0$, corresponding to the kinetic part and

$$S_2 = \begin{cases} \dot{\pi} = f(Q), \\ \dot{Q} = 0, \end{cases} \tag{7}$$

corresponding to the potential part, and the numerical scheme is

$$(\pi, Q)^{(j+1)} = \varphi_{h/2}^{[S_2]} \circ \varphi_h^{[S_1]} \circ \varphi_{h/2}^{[S_2]}((\pi, Q)^{(j)}), \quad j = 0, 1, \ldots,$$

where $\varphi_h^{[S_1]}$ and $\varphi_h^{[S_2]}$ represent the exact flows of S_1 and S_2.

The first equation in (6) is independent from the external force $f(Q)$, and is simply a free rigid body problem.

Rewriting the first part of system (6) in terms of the angular velocity, $\omega = T^{-1}\pi$, one obtains the Euler equations (1). We can compute $\pi(t)$, for any t and any initial value $\pi^{(j)}$, to machine accuracy by using the exact solution of the Euler equations, and computing the Jacobi elliptic integrals by the method of Arithmetic-Geometric mean, see section 3. Hence, the update of π, on the interval $[t_j, t_{j+1}]$,

$$\pi^{(j+1)} = Q(t_{j+1})\pi^{(j)}, \tag{8}$$

is "exact". However, $Q(t_{j+1})$ can not be directly deduced from the solution of the first equation in (6) and must be obtained by numerical integration of the second equation of (6). The approximation $Q^{(j+1)} \approx Q(t_{j+1})$ is obtained integrating numerically the equation

$$\dot{Q} = \text{skew}(T^{-1}\pi)\, Q, \quad Q(t_j) = I,$$

using a symmetric Magnus method (of order 2 or 4), [8]. For order 2 this results in the following expression

$$Q^{(j+1)} = \exp\left(\text{skew}\left(h\, T^{-1}\pi^{(j+1/2)}\right)\right), \tag{9}$$

where $\pi^{(j+1/2)} = \pi(t_j + h/2)$ is obtained as a by-product of the update $\pi^{(j+1)}$ in (8) with little extra cost (see section 3 for details). The exponential in (9) is computed by Rodrigues formula. Thus, the flow $\varphi_h^{[S_1]}$ is approximated by a second order flow $\phi_h^{[S_1]}$.

Given $f(Q^j)$ the flow $\varphi_h^{[S_2]}$ can be calculated exactly

$$\begin{aligned} \pi^{(j+1)} &= \pi^{(j)} + h f(Q^{(j)}), \\ Q^{(j+1)} &= Q^{(j)}, \end{aligned}$$

and the updating (second order) scheme is finally

$$(\pi^{(j+1)}, Q^{(j+1)}) = \varphi_{h/2}^{[S_2]} \circ \phi_h^{[S_1]} \circ \varphi_{h/2}^{[S_2]}((\pi^{(j)}, Q^{(j)})),$$

where

$$\phi_h^{[S_1]}((\pi^{(j)}, Q^{(j)})) = \begin{cases} \pi^{(j+1)} = Q(t_{j+1})\pi^{(j)}, \\ Q^{(j+1)} = \exp\left(\text{skew}\left(h\, T^{-1}\pi^{(j+1/2)}\right)\right), \end{cases} \tag{10}$$

$$\varphi_h^{[S_2]}((\pi^{(j)}, Q^{(j)})) = \begin{cases} \pi^{(j+1)} = \pi^{(j)} + h\, f(Q^{(j)}), \\ Q^{(j+1)} = Q^{(j)} \end{cases} \tag{11}$$

It is easy to verify that $\phi_h^{[S_1]}\phi_{-h}^{[S_1]} = I$ and the overall splitting method has the time-symmetry property,

$$\Phi_h \Phi_{-h} = 1, \quad \Phi_h = \varphi_{h/2}^{[S_2]} \circ \phi_h^{[S_1]} \circ \varphi_{h/2}^{[S_2]}.$$

3 Implementation issues

Starting form the Euler equations (1) and using the constants of motion (2), consider the values

$$\begin{aligned} a_1^2 &= 2EI_3 - G^2, \qquad a_3^2 = G^2 - 2EI_1, \\ b_1^2 &= I_2(I_3 - I_2), \qquad b_3^2 = I_2(I_2 - I_1). \end{aligned} \tag{12}$$

Assume $b_3/a_3 \le b_1/a_1$ (we will have a similar situation if $b_3/a_3 \ge b_1/a_1$), the solutions of the Euler equations are

$$\omega_1 = \frac{a_1 \,\text{cn}\, u}{\sqrt{I_1(I_3 - I_1)}}, \quad \omega_2 = \frac{a_1 \,\text{sn}\, u}{b_1}, \quad \omega_3 = \frac{a_3 \,\text{dn}\, u}{\sqrt{I_3(I_3 - I_1)}}, \tag{13}$$

where the Jacobi elliptic functions cn, sn and dn, are defined by

$$\operatorname{cn} u = \cos\varphi, \quad \operatorname{sn} u = \sin\varphi, \quad \operatorname{dn} u = \sqrt{1-k^2\sin^2\varphi}, \tag{14}$$

with $u(t) = \pm\lambda(t-\tau)$, $\lambda = b_1 a_3/(I_2\sqrt{I_1 I_3})$ and τ is a constant of integration which is used to satisfy the initial conditions. Here, the *amplitude* φ is given implicitly as the solution of the following equation

$$F(\varphi|k^2) = u(t), \tag{15}$$

where

$$F(\varphi|k^2) := \int_0^{\varphi} \frac{d\theta}{\sqrt{1-k^2\sin^2\theta}}$$

is an elliptic integral of the first kind with modulus $k = b_3 a_1/(b_1 a_3)$. For each integration step, as described in the previous section, we have to calculate the exact solution $\omega^{(j+1)} := \omega(t_j+h)$ and $\omega^{(j+c_i)} := \omega(t_j+c_i h)$, $c_i \in (0,1)$, of a free rigid body problem with the initial condition $\omega(t_j) = \omega^{(j)}$, computed at the previous time step. For this purpose we compute the values of

$$\operatorname{sn} u = \sin\varphi, \quad \operatorname{cn} u = \cos\varphi, \quad \operatorname{dn} u = \sqrt{1-k^2\sin^2\varphi},$$

to machine accuracy for a given input $u = \lambda(t-\tau)$. In practice the vector of times $(t_j + c_i h, t_j + h)^T$ is used to calculate simultaneously the amplitudes $\varphi^{(j+c_i)}$, $\varphi^{(j+1)}$, with respect to the same initial condition. Here λ and k are given, except for the sign.

The first task of the process is to determine the appropriate τ to satisfy the initial condition $\omega(t_j) = \omega^{(j)}$. To this end, we first find the amplitude $\varphi^{(j)} \in [0, 2\pi]$, which is uniquely determined from the equations

$$\omega_1(t_j) = \frac{a_1\cos\varphi^{(j)}}{\sqrt{I_1(I_3-I_1)}}, \quad \omega_2(t_j) = \frac{a_1\sin\varphi^{(j)}}{b_1}.$$

Furthermore, from the sign of $\omega_3(t_j)$,

$$\omega_3(t_j) = \frac{a_3\sqrt{1-k^2\sin^2\varphi^{(j)}}}{\sqrt{I_3(I_3-I_1)}},$$

we determine the sign of the constants a_3 and λ. Now we compute τ from (15) and we have

$$\tau = t_j - \frac{1}{\lambda}F(\varphi^{(j)}|k^2) \tag{16}$$

where

$$F(\varphi^{(j)}|k^2) = \int_0^{\varphi^{(j)}} \frac{d\theta}{\sqrt{1-k^2\sin^2\theta}}. \tag{17}$$

The latter integral can be computed to the desired accuracy using the method of Arithmetic-Geometric Mean. We consider the sequence $\{\varphi_n^{(j)}\}_{n=0,1,\ldots}$, $\varphi_{n+1}^{(j)} > \varphi_n^{(j)}$, defined by

$$\tan(\varphi_{n+1}-\varphi_n) = \frac{b_n}{a_n}\tan\varphi_n, \quad \varphi_0 = \varphi^{(j)},$$

where a_n, b_n are given by the Arithmetic-Geometric Mean sequence, [1], i.e.

$$a_{n+1} = \frac{a_n+b_n}{2}, \quad b_{n+1} = \sqrt{a_n b_n}, \quad c_{n+1} = \frac{a_n-b_n}{2}.$$

The iteration stops when $n = N$ and c_N is less than tolerated error, the initial values are

$$a_0 = 1, \quad b_0 = \sqrt{1-k^2}, \quad c_0 = k.$$

One can show that

$$F(\varphi_0|k^2) = \lim_{n\to\infty} \frac{\varphi_n}{2^n a_n}, \quad \varphi_0 = \varphi^{(j)}. \tag{18}$$

As the Geometric-Arithmetic Mean sequence converges quadratically, one obtains accurate approximations of $F(\varphi^{(j)}|k^2)$ in very few recursion steps. From (16) we easily obtain τ. In our implementation we terminate the iteration when c_N is less then machine epsilon.

Now to find the solution of the Euler equations at the desired time values we consider $(u^{(j+c_i)}, u^{(j+1)})^T = (\lambda(t^{(j+c_i)} - \tau), \lambda(t^{(j+1)} - \tau))^T$, we substitute in (15), and we get the values of the elliptic integrals for the amplitudes $(\varphi^{(j+c_i)}, \varphi^{(j+1)})^T$.

To recover the values of the amplitudes we use (18) with

$$\varphi_0 = \varphi^{(j+c_i)}, \quad \varphi_0 = \varphi^{(j+1)},$$

and find φ_0 by recursion. We start at $\varphi_N \approx 2^N a_N F(\varphi_0|k^2)$, and apply the transformation

$$\sin(2\varphi_{n-1} - \varphi_n) = \frac{c_n}{a_n}\sin\varphi_n, \qquad \varphi_n^{(j+c_i)} > \varphi_{n-1}^{(j+c_i)}, \quad \varphi_n^{(j+1)} > \varphi_{n-1}^{(j+1)},$$

for $n = N, N-1, \ldots, 0$.

The described procedure, to calculate φ to desired accuracy for u and k^2 given, can be performed in MATLAB by the function `ellipj`. Our implementation is slightly more efficient as it computes the Arithmetic-Geometric mean just once for each time-step of the splitting algorithm.

Note that φ, from the relation (17), can be found explicitly for the special cases $k^2 = 1$ or $k^2 = 0$.

4 Numerical experiments

The splitting method proposed in this paper is compared with the symplectic method of [2] and [16] which we denote in short by MR, with the Discrete Moser-Veselov methods of [13] (DMV), and with the classical fourth order Runge-Kutta method (RK4). We also refer to the second order symmetric splitting method, described in the previous section, as SEJ. The symplectic method MR is based on a splitting of the the Hamiltonian $\mathcal{H}$ into four parts,

$$\tilde{\mathcal{H}}_1 = \frac{\pi_1^2}{2I_1}, \quad \tilde{\mathcal{H}}_2 = \frac{\pi_2^2}{2I_2}, \quad \tilde{\mathcal{H}}_3 = \frac{\pi_3^2}{2I_3}, \quad \tilde{\mathcal{H}}_4 = V(Q).$$

Each of the corresponding Hamiltonian vector fields can be integrated exactly ($\tilde{\mathcal{H}}_1$, $\tilde{\mathcal{H}}_2$, $\tilde{\mathcal{H}}_3$ correspond to the vector fields (3)), the symmetric composition of the flows gives rise to the approximation scheme,

$$(\pi, Q)^{(j+1)} = \Phi_M((\pi, Q)^{(j)}),$$

where

$$\Phi_M = \varphi_{4,h/2} \circ \Phi_{T,h} \circ \varphi_{4,h/2}.$$

Here

$$\Phi_{T,h} = \varphi_{1,h/2} \circ \varphi_{2,h/2} \circ \varphi_{3,h} \circ \varphi_{2,h/2} \circ \varphi_{1,h/2}$$

is the contribution from the kinetic parts, $\tilde{\mathcal{H}}_1$, $\tilde{\mathcal{H}}_2$ and $\tilde{\mathcal{H}}_3$. The flows of kinetic parts correspond to elementary rotations in $\mathbf{R}^3$. For example for $\mathcal{H}_1$

$$\varphi_{1,h}((\pi,Q)^{(j)}) = \begin{cases} \pi^{(j+1)} = R_x(h)\pi^{(j)}, \\ Q^{(j+1)} = R_x(h), \end{cases}$$

where

$$R_x(h) = \begin{pmatrix} 1 & 0 & 0 \\ 0 & \cos(C^{(j)}h) & \sin(C^{(j)}h) \\ 0 & -\sin(C^{(j)}h) & \cos(C^{(j)}h) \end{pmatrix},$$

and

$$C^{(j)} = \frac{\pi_1^{(j)}}{2I_1}.$$

While the flow for $\tilde{\mathcal{H}}_4$ is the same as for the system S_2 (5) of the previous section, i.e. $\varphi_{4,h} = \varphi_h^{[S_2]}$.

4.1 Free rigid body experiments

In the first experiment we consider the integration of the FRB. In this experiment we perform a comparison also with the DMV methods. We refer to [13] and [15] for a detailed description of these methods, and recall that the higher order DVM are obtained by computing appropriate rescaling of the initial condition. In figure 1 we plot on the *x* axis the number of floating point operations required by the methods to perform the integration on the interval $[0,1]$, for different choices of the step size. On the *y* axis we report the corresponding values of the 2-norm of the global error. In all the experiments the reference solution for computing the global error is obtained using the built in function of MATLAB, `ode45`, setting the absolute and relative tolerance equal to $10e-14$. The MR method in this case involves the computation of the three flows corresponding to the Hamiltonians $\tilde{\mathcal{H}}_1$, $\tilde{\mathcal{H}}_2$, $\tilde{\mathcal{H}}_3$ only. The SEJ method produces a very accurate solution of the problem (the error is of the size of 10^{-14}) and the error is independent on the step size of integration. The MR and DMV methods of order 2 and 4 perform similarly with a slight advantage for the MR in the second order case and of DVM in the fourth order case. It is plausible that the advantage for DMV is even bigger in the sixth order case.

With about the same amount of floating point operations the MR and DMV methods produce a much pourer approximation of the solution compared to SEJ, in this case the accuracy depends on the step size and increases with the number of floating point operations. In this experiment the principal moments of inertia and the initial value for ω are $I_1 = 5$, $I_2 = 4$, $I_3 = 3$ and $\omega_0 = (1,0,2)^T$. The cost for computing the rescaling factors in the DMV methods and for the computation of τ in SEJ are not included in this experiment.

In the second experiment we perform the numerical integration of a FRB with the same moments of inertia and the same initial value of the first experiment, on the interval $[0,400]$. In figure 2 we consider the energy error as the difference between the constant exact energy, given by $\mathcal{H}$, and the energy obtained from the numerical methods (with step size $h = 0.4$). We note that for the Runge-Kutta method there is a visible energy drift, for the MR of order 2 and 4 method we observe a typical behavior of symplectic methods, i.e. the energy error is oscillating near zero, (the amplitude of the oscillations is about 10^{-3} for order 2, and about 10^{-5} for the order 4 method). The DMV methods give an energy error of the size of

10^{-13}, and the method based on the use of the Jacobi elliptic functions, SEJ, computes a very accurate solution of the FRB problem and the energy is conserved to the same accuracy (the energy error is about 10^{-16}).

4.2 Heavy top experiments

In figure 3 we report the results of the third experiment. We consider the integration of the heavy top problem which corresponds to taking

$$V(Q) = e_3^T Q u_0,$$

where e_3 is the third canonical vector and u_0 is the initial position of the center of mass of the heavy top. This gives rise to a torque in (5) of the form

$$f(Q) = \begin{bmatrix} u_2 \\ -u_1 \\ 0 \end{bmatrix}, \quad u(t) = Q(t)u_0.$$

We use the splitting methods MR and SEJ on the interval $[0,1]$. The principal moments of inertia are $I_1 = 0.1$, $I_2 = 1$, $I_3 = 10$, and $\omega_0 = (3,3,3)^T$ and $u_0 = (0,0,1)^T$, respectively.

We first integrate on the interval $[0,1]$ and compare the performance of the two splitting methods in terms of floating point operations against global error, figure 3, in this case the advantage of the new splitting method is quite clear.

Next we illustrate the qualitative performance of the two methods by comparing the results obtained by using different step sizes. We look at the energy error and the numerical trajectory describing the motion of center of mass, in figures 4 and 5. For step size $h = 0.01$ the two methods produce similar trajectories (the norm $\|u_{\mathrm{SEJ}} - u_{\mathrm{MR}}\| = O(10^{-1})$). The energy error for SEJ is a factor 10^{-3} smaller than for MR. Increasing the step size to $h = 0.02$ and $h = 0.04$, the amplitude of the oscillations in the energy error increases for both methods. Consistently for all the experiments, SEJ has much smaller energy error than MR. For $h = 0.02$ the trajectory of the center of mass produced by the MR method is quite different from the one produced with step size $h = 0.01$, and it becomes completely chaotic for $h = 0.04$. For the SEJ method the numerical trajectory of the center of mass preserve the same qualitative behavior for $h = 0.01$, $h = 0.02$ and $h = 0.04$, figure 4.

Next, we compare the energy error between the two methods for different values of the inertia tensor. The initial conditions for the angular velocity and the position of the center of mass are chosen $\omega_0 = (3,3,3)$ and $u_0 = (0,0,1)$. The energy error is measured when I_1 and I_2 are held fixed at $I_1 = 0.1, I_2 = 0.2$ and $I_1 = 0.1, I_2 = 5$, respectively, while I_3 is varying between $I_2 < I_3 < 10$. Studying the two graphs in figure 6 it appears that the energy error for the SEJ method is generally lower than for the MR method, in particular when the inertia is significantly larger in one direction (I_3) and the body is strongly asymmetric.

4.3 Satellite experiments

We consider the motion of a satellite in a circular orbit of radius r around the earth. The frame of reference centered in the center of the earth is called $\mathcal{F}_c$. The orthogonal matrix Q represents the rotation of the fixed body frame, ($\mathcal{F}_b$), with respect to $\mathcal{F}_c$. The third canonical vector e_3 is aligned with the vector pointing from the center of $\mathcal{F}_c$ to the center of $\mathcal{F}_b$. The canonical vector e_1 is aligned with the tangent to the circular orbit at the origin of $\mathcal{F}_b$, and $e_2 = e_3 \times e_1$, and $\times$ denotes the usual vector cross product. Consider $\mu = GM$ where G is

the gravitational constant and M is the mass of the earth, then the potential energy of the problem is given by

$$V(Q) = 3\frac{\mu}{2r^3}(Qe_3)^T TQe_3,$$

T is the inertia tensor. The torque $f(Q)$ in equations (5) is here given by

$$f(Q) = 3\frac{\mu}{r^3}(Qe_3) \times (TQe_3).$$

Here after we indicate with SEJ4 the second order symmetric splitting method where the rotation matrix Q is approximated with a 4th order symmetric Magnus method, while for the method SEJ the rotation matrix Q is approximated with a second order Magnus method as in (9).

In the first experiment on the satellite model we compare the methods MR, SEJ and SEJ4. The inertia moments are chosen to be

$$I_1 = 1.7 \times 10^4, \quad I_2 = 3.7 \times 10^4, \quad I_3 = 5.4 \times 10^4,$$

the initial condition for the angular velocity is

$$\omega_0 = (15, -15, 15)^T,$$

and $Q(0) = I$ (the identity matrix). We have $\mu = GM = 3.986 \times 10^{14}$, $r = 1.5 \times 10^5$. We integrate on the interval $[0, 400]$ for two different step sizes $h = 0.1$ and $h = 0.05$. In figure 7, the step size is $h = 0.1$. Figures 7 (a), (c), (e) in the left column illustrate the qualitative performance of the three methods for the vector Qe_3. The method SEJ4 gives the best results.

In the right column of figure 7, the energy error for the three methods is presented. Both SEJ and SEJ4 preserve the energy much better than the MR method.

In figure 8, the step size is $h = 0.05$. Here the qualitative behavior seams to be almost identical for the three different methods. Similarly to the previous case the SEJ methods give better energy preservation compared to MR.

In some of the presented experiments we have considered different orderings of the elementary flows which define the MR methods, this has not given significant differences in the results. An analysis of how different compositions of the flows can influence the size of the enrgy error can be found in [5]. We do not exclude that appropriate orderings of the flows can give improved performance for the MR splitting in some cases.

5 Conclusions

In this paper we presented a symmetric splitting method for the integration of rigid body problems subject to external forces. The numerical strategy is based on the use of available efficient algorithms for the computation of Jacobi elliptic functions. We compared the method with a similar symplectic splitting method of [16] and [2]. In many of the performed experiments the presented symmetric splitting is more efficient then the symplectic splitting, giving smaller global error for the same amount of floating point operations. Moreover the new method presents in many experiments a better energy conservation. This seems to be true especially for problems where the principal moments of inertia are very different in size.

6 Acknowledgments

The authors are grateful to Brynjulf Owren for promoting the use of the exact solution of the FRB equations in numerical integrators, and to Antonella Zanna for useful discussions, and for providing the codes with the implementation of the Discrete Moser Veselov algorithms of [13].

References

[1] *Handbook of mathematical functions with formulas, graphs, and mathematical tables*, volume 55 of *National Bureau of Standards Applied Mathematics Series, 55*. Reprint of the 1972 edition. Dover Publications, Inc., New York, 1992.

[2] R. McLachlan A. Dullweber, B. Leimkuhler. Symplectic splitting methods for rigid body molecular dynamics. *J. Chem. Phys.*, 107:5840–5851, 1997.

[3] J. Butcher. *Numerical Methods for Ordinary Differential Equations*. Wiley, second edition edition, 2003.

[4] E. Celledoni and B. Owren. Lie group methods for rigid body dynamics and time integration on manifolds. *Comput. Methods Appl. Mech. Engrg.*, 192:421–438, 2003.

[5] F. Fasso'. Comparison od splitting algorithms for the rigid body. *Journal of Computational Physics*, 189:527–538, 2003.

[6] Z. Ge and J.E. Marsden. Lie-Poisson Hamilton-Jacobi theory and Lie-Poisson integrators. *Physics Letters A*, 133(3):134–139, 1988.

[7] M. Geradin and A. Cardona. *Flexible Multibody Dynamics*. Wiley and Sons Ltd., 2001.

[8] E. Hairer, C. Lubich, and G. Wanner. *Geometric numerical integration*, volume 31 of *Springer series in compuitational mathematics*. Springer, 2002.

[9] B. Leimkuhler and S. Reich. *Simulating Hamiltonian Dynamics*, volume 14 of *Cambridge Monographs on Applied and Computational Mathematics*. Cambridge University Press, first edition edition, 2004.

[10] D. Lewis and J. C. Simo. Conserving algorithms for the dynamics of Hamiltonian systems of Lie groups. *J. Nonlinear Sci.*, 4:253–299, 1994.

[11] J. E. Marsden and T. S. Ratiu. *Introduction to Mechanics and Symmetry*. Springer-Verlag, 1994.

[12] R. I. McLachlan. Explicit Lie-Poisson integration and the Euler equations. *Physical Review Letters*, 71:3043–3046, 1993.

[13] R. I. McLachlan and A. Zanna. The discrete Moser–Veselov algorithm for the free rigid body, revisited. *Found. of Comp. Math.*, 5(1):87–123, 2005.

[14] J.Wm. Mitchell. *A simplified variation of parameters solution for the motion of an arbirarily torqued mass asymmetric rigid body*. PhD thesis, University of Cincinnati, 2000.

[15] J. Moser and A. Veselov. Discrete versions of some classical integrable systems and factorization of matrix polynomials. *J. of Comm. Math. Phys.*, 139(2):217–243, 1991.

[16] S. Reich. Symplectic integrators for systems of rigid bodies. Integration algorithms and classical mechanics (Toronto, ON, 1993). *Fields Inst. Commun.*, 10:181–191, 1996.

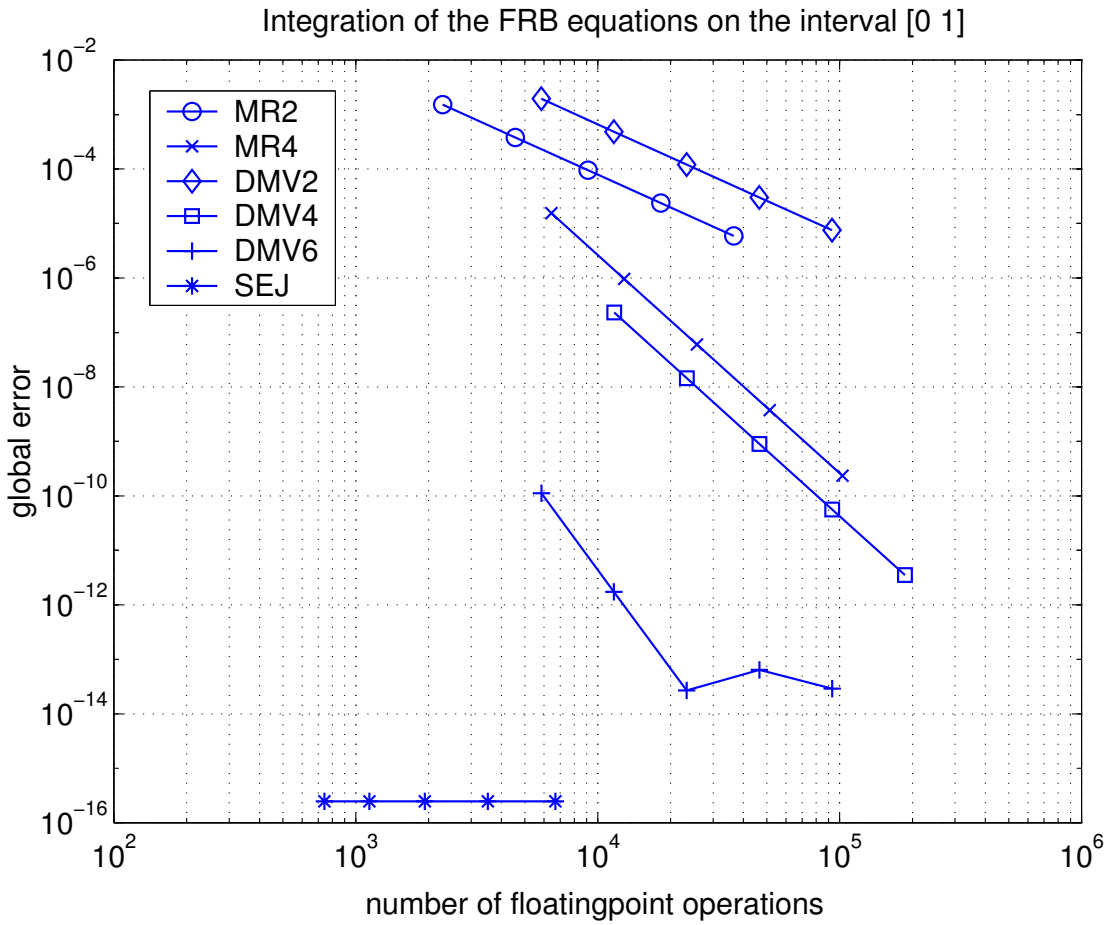

Figure 1: Free rigid body. Number of floating point operations against the global error. Integration on the interval $[0, 1]$ with different step sizes. The methods are: MR of order 2 and 4, DMV of order 2, 4 and 6, and the method SEJ based on the accurate computation of the Jacobi elliptic functions.

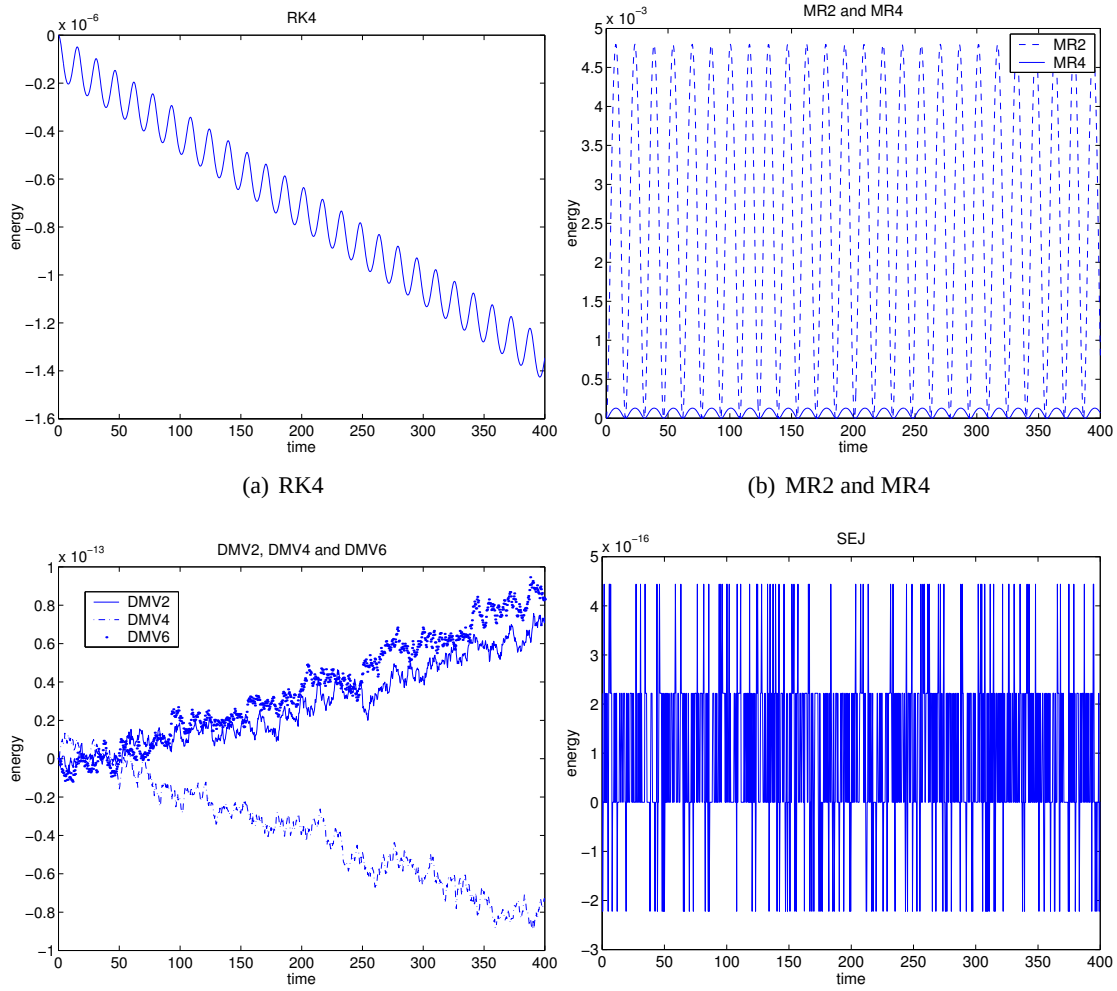

(a) RK4 (b) MR2 and MR4

(c) DMV2 and DMV4 (d) SEJ

Figure 2: Energy error for the numerical integration of the free rigid body equations. Integration on the interval $[0, 400]$.

Figure 3: Heavy top. Number of floating point operations against the global error. Integration on the interval $[0,1]$ with different step sizes.

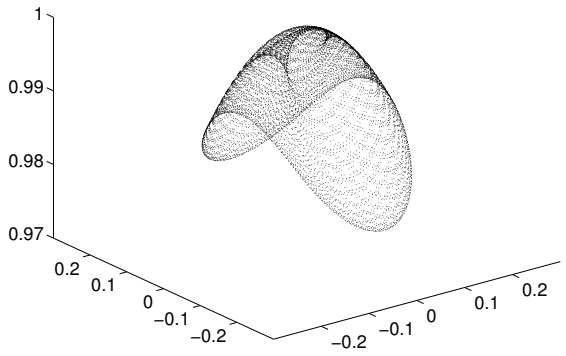

(a) Center of mass u, $h = 0.01$, SEJ

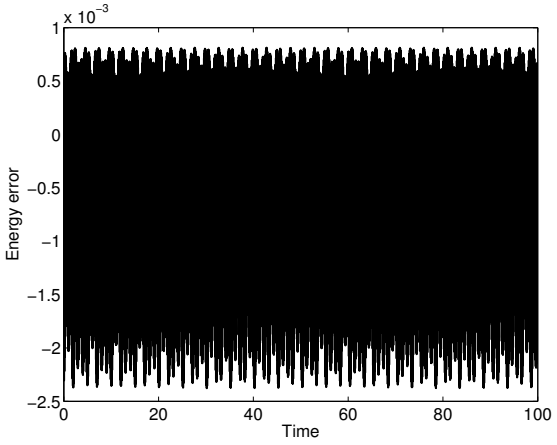

(b) SEJ, $h = 0.01$

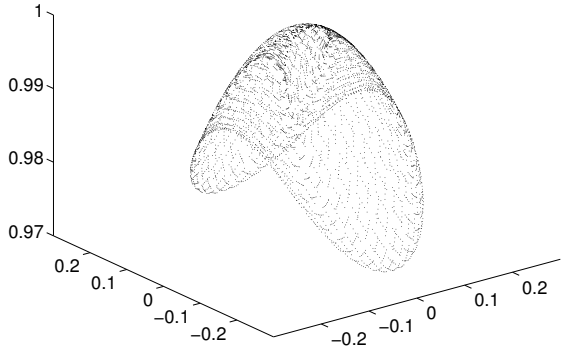

(c) Center of mass u, $h = 0.02$, SEJ

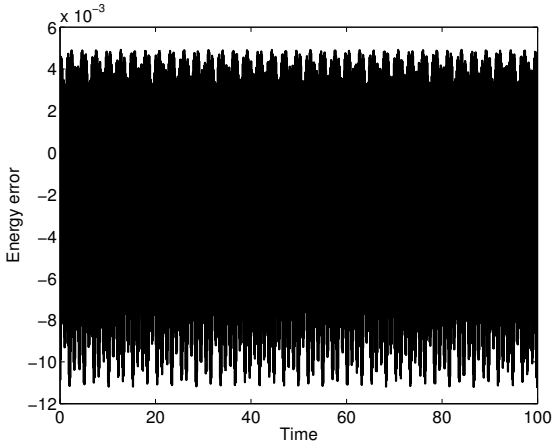

(d) SEJ, $h = 0.02$

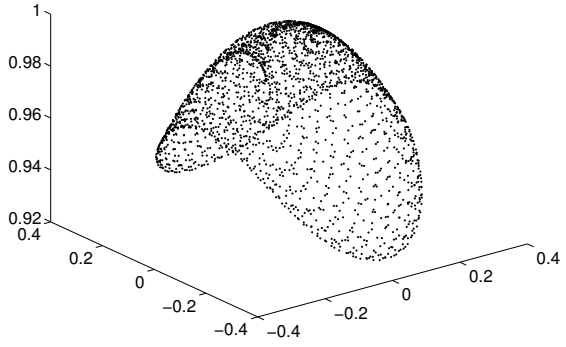

(e) Center of mass u, $h = 0.04$, SEJ

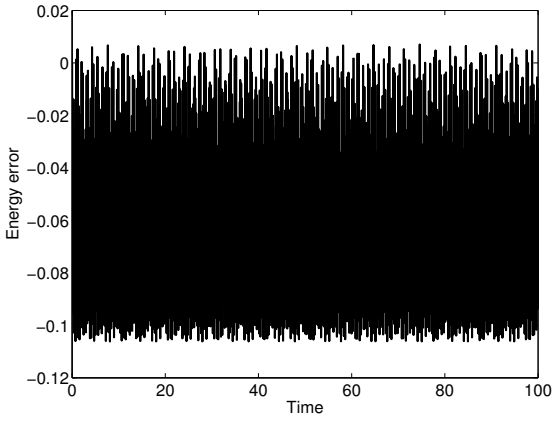

(f) SEJ, $h = 0.04$

Figure 4: Energy error for the heavy top. Integration on the interval $[0, 100]$, using the method SEJ.

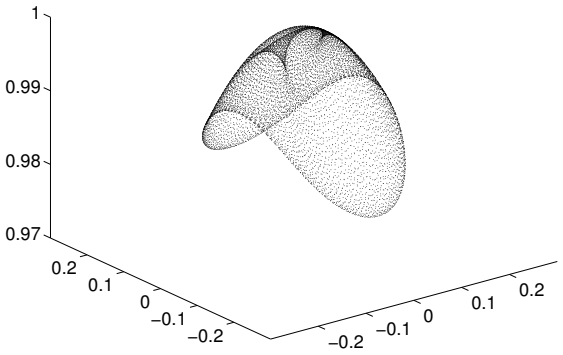

(a) Center of mass u, $h = 0.01$, MR

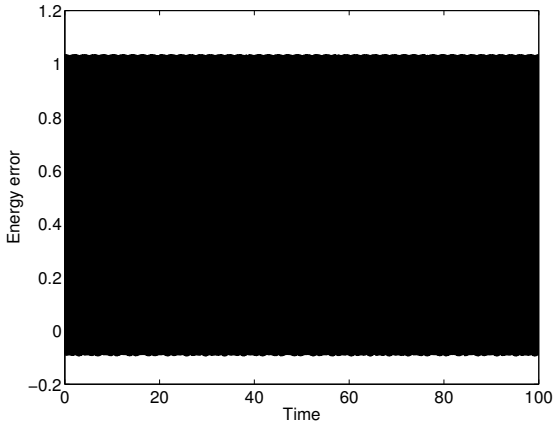

(b) MR, $h = 0.01$

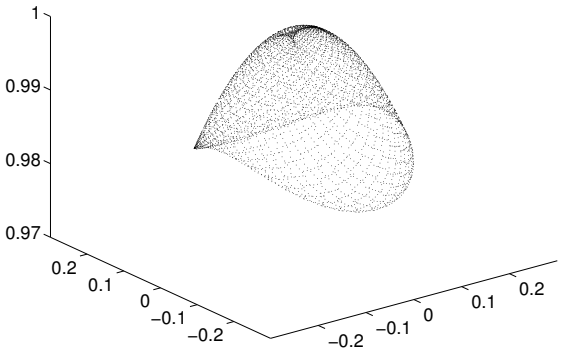

(c) Center of mass u, $h = 0.02$, MR

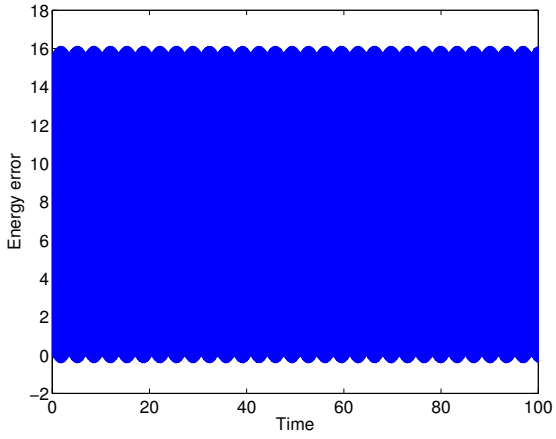

(d) MR, $h = 0.02$

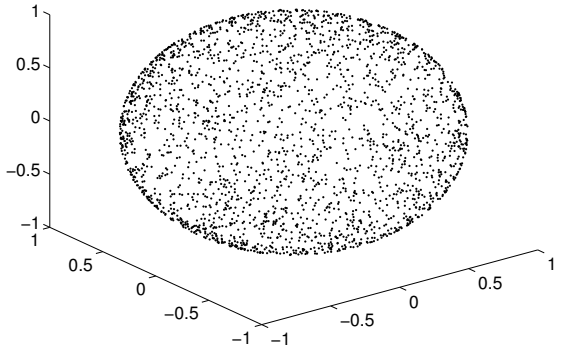

(e) Center of mass u, $h = 0.04$, MR

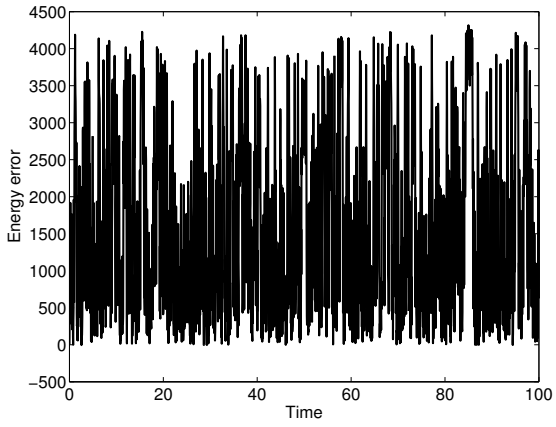

(f) MR, $h = 0.04$

Figure 5: Energy error for the heavy top. Integration on the interval $[0, 100]$, using the method MR.

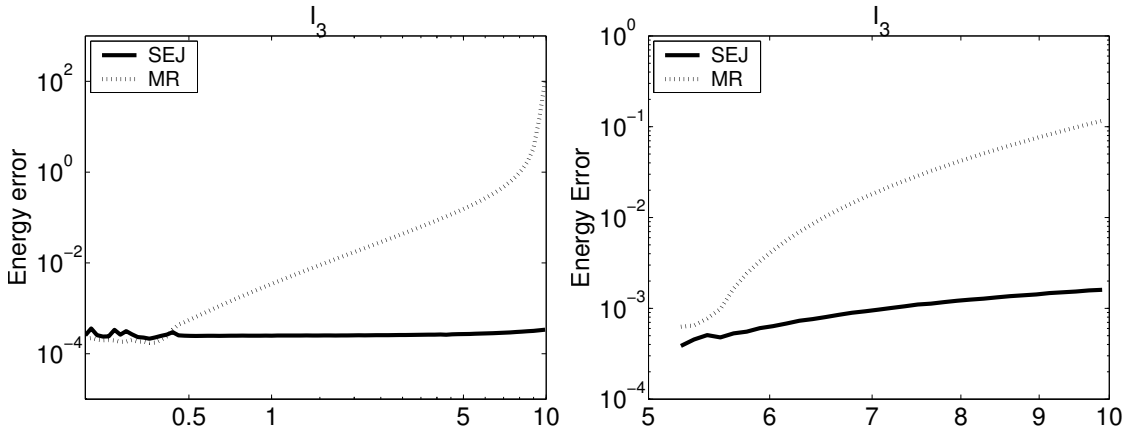

(a) $I_1 = 0.1, I_2 = 0.2$ (b) $I_1 = 0.1, I_2 = 5$

Figure 6: Energy error for the heavy top. Integration on the interval $[0,10]$, $h = 0.01$, using different inertia tensors. I_2 and I_3 are varying, while $I_1 = 0.1$ is held fixed. In 6(a) $I_2 = 0.2$. In 6(b) $I_2 = 5$.

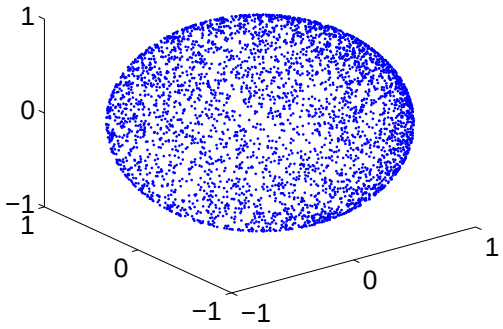

(a) Body frame Qe_3, $h = 0.1$, MR

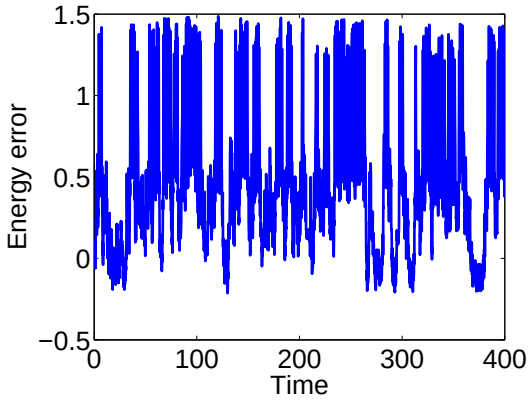

(b) Energy error MR, $h = 0.1$

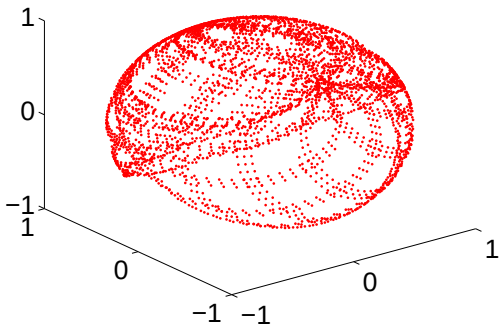

(c) Body frame Qe_3, $h = 0.1$, SEJ

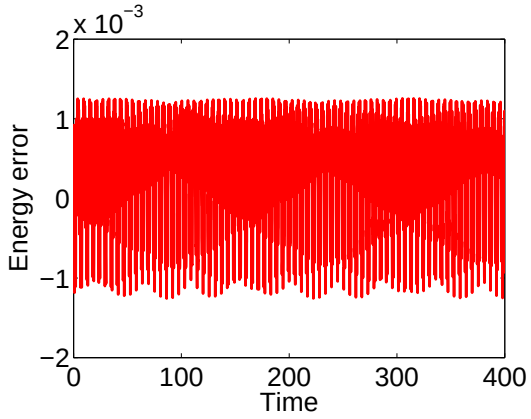

(d) Energy error SEJ, $h = 0.1$

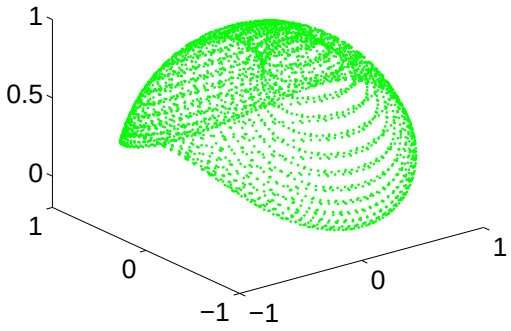

(e) Body frame Qe_3, $h = 0.1$, SEJ4

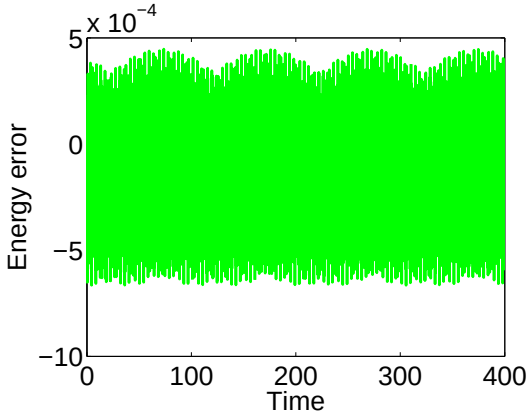

(f) Energy error SEJ4, $h = 0.1$

Figure 7: Plot of Qe_3 and the energy error for the satellite simulation. Integration on the interval $[0, 400]$, using the method MR, SEJ and SEJ4 (SEJ with 4^{th} order approximation of the rotation matrix Q).

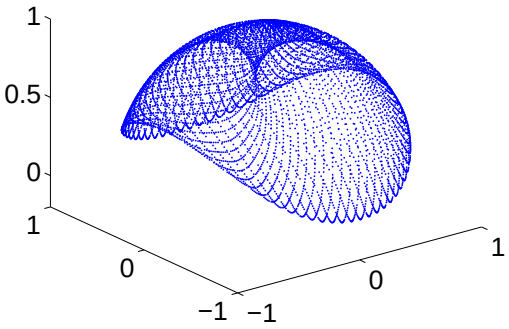

(a) Body frame Qe_3, $h = 0.05$, MR

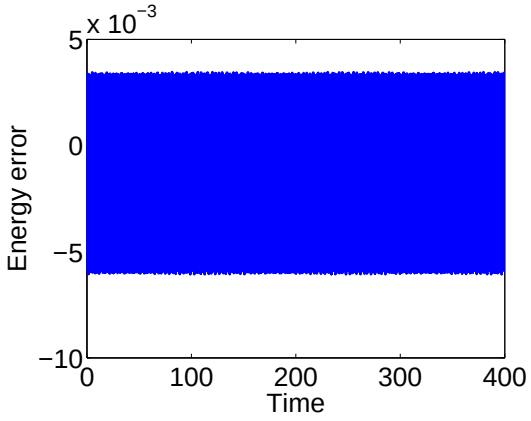

(b) Energy error MR, $h = 0.05$

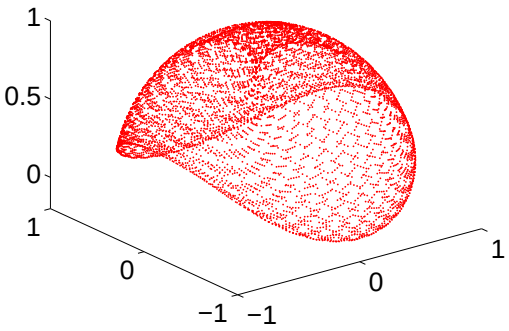

(c) Body frame Qe_3, $h = 0.05$, SEJ

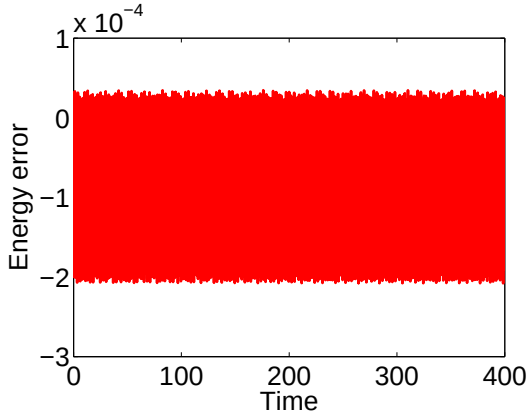

(d) Energy error SEJ, $h = 0.05$

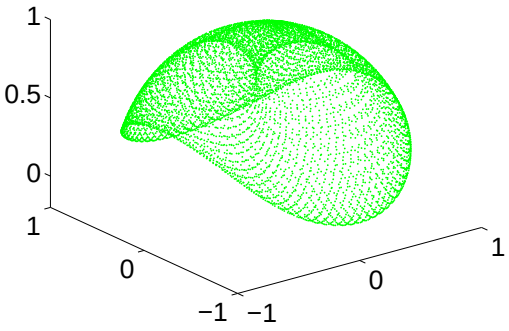

(e) Body frame Qe_3, $h = 0.05$, SEJ4

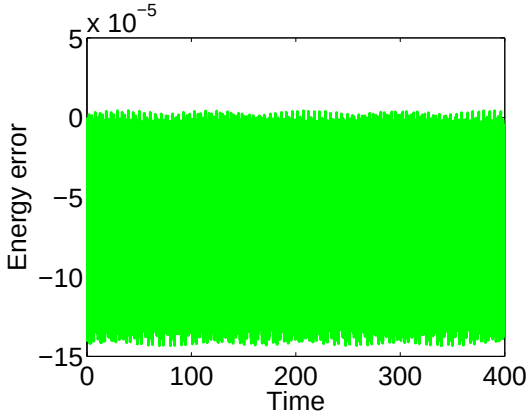

(f) Energy error SEJ4, $h = 0.05$

Figure 8: Plot of Qe_3 and the energy error for the satellite simulation. Integration on the interval $[0, 400]$, using the method MR, SEJ and SEJ4 (SEJ with 4^{th} order approximation of the rotation matrix Q).